

Semiconductors

Benzimidazole Derivatives: Synthesis, Physical Properties, and n-Type Semiconducting Properties

Masashi Mamada,^[a, b] César Pérez-Bolívar,^[a] Daisuke Kumaki,^[b] Nina A. Esipenko,^[a] Shizuo Tokito,^[b] and Pavel Anzenbacher, Jr.*^[a]

Abstract: A series of new benzimidazole derivatives were synthesized by the solid-state condensation and direct sublimation (SSC-DS) method and their physical properties were investigated. The reaction yields and product stability were significantly affected by the identity of the diamine and anhydride substituents. On the other hand, the substituents of the benzimidazole ring allowed fine tuning of the emission maxima, fluorescence quantum yields, and redox potentials. The HOMO–LUMO levels were estimated by cyclic voltam-

metry in film on indium tin oxide (ITO) and compared with values obtained by other methods. The described benzimidazoles showed high crystallinity, which is attributed to a high planarity and interactions between carbon and heteroatoms. These compounds showed n-type semiconducting behavior in organic field-effect transistors (OFETs). Optimized devices for fluorinated NTCBI (naphthalene tetracarboxylic bisbenzimidazole) showed respectable electron mobilities of $\sim 10^{-2} \text{ cm}^2 \text{ V}^{-1} \text{ s}^{-1}$.

Introduction

Perylene and naphthalene benzimidazoles derived from perylene-3,4,9,10-tetracarboxylic acid and naphthalene-1,4,5,8-tetracarboxylic acid are important classes of dyes and pigments, and because of their semiconductor properties combined with high stability are potentially useful for applications in organic electronics. Perylene tetracarboxylic acid diimide (PDI) derivatives (Figure 1) have been known as vat dyes since the early 1900s.^[1] These pigments exhibit high chemical and heat stability, excellent light-fastness, and are used in high grade industrial paints, for example, in automotive applications. Currently, PDIs find utility in a wide-range of applications,^[2] especially in organic

electronics, including organic field-effect transistors (OFETs),^[3] and organic photovoltaics (OPVs).^[4] PDIs generally work as n-type semiconductors as they are able to form stable radical anions. Perylene tetracarboxylic acid bisbenzimidazole (PTCBI) is also well known in organic electronics as it was used in the first organic thin-film solar cell.^[5] PTCBI offers the advantage of a low energy gap and absorption over the whole UV/Vis ab-

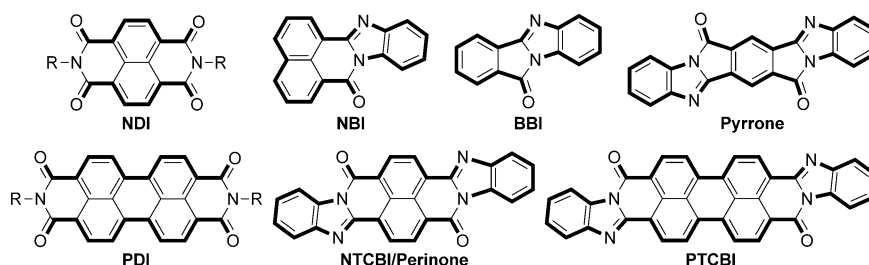


Figure 1. Chemical structures of carboxylic acid imido derivatives and carboxylic acid benzimidazole derivatives.

[a] Dr. M. Mamada, Dr. C. Pérez-Bolívar, Dr. N. A. Esipenko, Prof. Dr. P. Anzenbacher, Jr.
Department of Chemistry and Center for Photochemical Sciences
Bowling Green State University
Bowling Green, Ohio 43403 (USA)
Fax: (+1) 419-372-9809
E-mail: pavel@bgsu.edu

[b] Dr. M. Mamada, Dr. D. Kumaki, Prof. Dr. S. Tokito
Research Center for Organic Electronics
Graduate School of Science and Engineering
Yamagata University
4-3-16 Jonan, Yonezawa-shi, Yamagata 992-8510 (Japan)
Fax: (+81) 238-26-3788

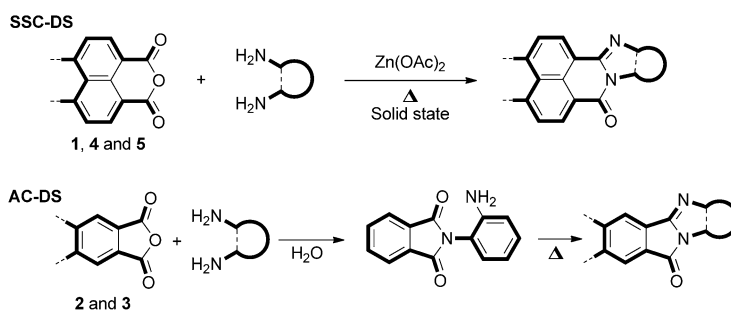
Supporting information for this article is available on the WWW under <http://dx.doi.org/10.1002/chem.201403058>.

sorption spectral region. With few exceptions,^[6] benzimidazoles of carboxylic acids have been less investigated. For example, naphthalene tetracarboxylic acid bisbenzimidazole (NTCBI), a widely used pigment called perinone, is only very rarely used in the organic electronics applications.^[7] On the other hand, owing to their high electron mobilities, naphthalene tetracarboxylic acid diimide (NDI) derivatives are among the most attractive candidates for n-type semiconductors.^[8] Presumably, the reason for less attention being paid to benzimidazole derivatives is their low solubility in organic solvents. To alleviate these problems, unsymmetrical materials with an imido moiety on one end and benzimidazole moiety on the other were developed.^[9] However, benzimidazoles such as PTCBIs and

NTCBIs are still less developed and there is no data regarding their substituted derivatives. The same is true for the naphthalene benzimidazoles (NBIs) that could be considered as a half unit of PTCBIs and that are potentially interesting chromophores.^[10] Thus, this study is focused on the synthesis and evaluation of properties of a series of PTCBI and NTCBI derivatives, their model compounds, such as NBI, and the benzene benzimidazole analogues (BBI).

Benzimidazole semiconductor derivatives were traditionally synthesized by heating at reflux in high-boiling solvents such as acetic acid, dimethylnaphthalene, imidazole, or quinoline in the presence of a Lewis acid. Recently, the NTCBI and PTCBI materials were prepared by using a solvent-free "green" process based on heating carboxylic acid anhydrides and arylene diamines in the presence of zinc acetate in the solid state followed by direct sublimation of the pure product.^[11] Here, we report the synthesis of a series of benzimidazole semiconductors bearing various substituents synthesized in a similar manner. In addition, physical properties including UV/Vis absorption, photoluminescence, electrochemistry, and crystal structures were investigated. Finally, we fabricated OFET devices for some of these materials to evaluate their electron-transporting properties.

First, the reactions between anhydrides **1–5** with 1,2-diaminobenzene, **a**, were investigated as the model reactions (Scheme 1). Several protic and Lewis acids were considered, including acetic and *p*-toluenesulfonic acids, imidazole (both as a catalyst and solvent), and various Zn^{II} and Al^{III} salts. It was concluded that zinc acetate catalyzes the solid-state condensation and direct sublimation (SSC-DS) for **1**, **4**, and **5**. However, for **2** and **3**, aqueous condensation conditions followed by direct sublimation (AC-DS) (Scheme 1) provided the best results. Following the test reactions, a variety of diamines with a wide range of functional groups were utilized.



Scheme 1. Synthesis of benzimidazole derivatives.

Results and Discussion

Synthesis of benzimidazole derivatives

Benzimidazole derivatives were synthesized from dicarboxylic acid anhydrides and diamines (Figure 2). The compounds derived from the combination of **1–5** and **a–d** were synthesized by the solid-state condensation and direct sublimation (SSC-DS) method recently developed by our group.^[11] This circumvented the typical condensation reactions performed under reflux in AcOH or high-boiling solvents as well as the column chromatography process for which the mobile phases contain trifluoroacetic acid (TFA).^[12] Furthermore, a new aqueous method, AC-DS, based on condensation in water followed by direct sublimation was also developed.

The reactions between **1** and diamines under SSC-DS conditions gave products in good yields (~80%). The exceptions were 3,4-diaminothiophene, **l**, and 4,5-diaminopyrene, **n**, (Table 1) presumably owing to the instability of these diamines. Note that 2,5-disubstituted-3,4-diaminothiophenes have better stability than compound **l**, resulting in higher yields for the condensation reactions.^[9] SSC-DS of **1l** with zinc acetate gave only a small amount of product (~10%). Further investigation revealed that the reaction proceeds via the imide intermediate **6**. The imide derivative **6** was then synthesized from compound **1** and diamine **l** by heating at 60 °C in EtOH as shown in Scheme 2. The imido compound **6** was relatively stable (compared with diamine **l**) at 200 °C giving a trace amount of product **1l**. Similarly, heating of **6** in the presence of zinc acetate gave only a small amount of product. On the other hand, the imide compound **6** could be condensed at 200 °C with imidazole in moderate yield (~70%). Thus, imidazole appears to be a suitable solvent for the condensation of 3,4-diaminothiophene with carboxylic anhydrides.

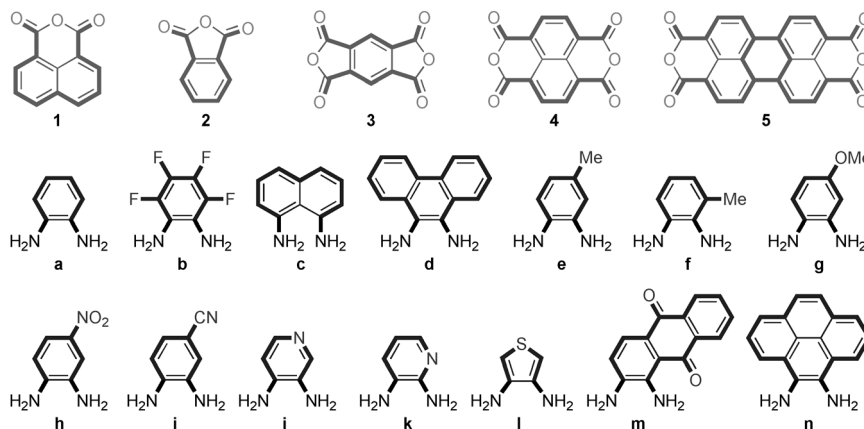


Figure 2. Chemical structures of starting materials.

In the reaction between compound **1** and **n**, the crude product consisted of unreacted **1** (sublimed at lower temperature), the expected product **1n** and dipyrro[4,5-*b*:4',5'-*e*]pyrazine, **8**, sublimed at a relatively

Table 1. The reaction yields of condensation products after sublimation, photophysical and electrochemical properties, and estimated HOMO–LUMO energies.

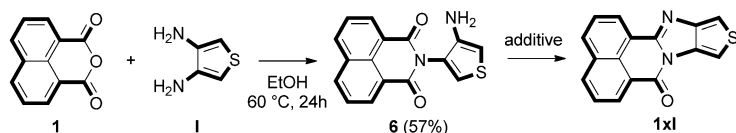
Compound	Yield [%]	Solution ^[g]		Film		Solution		DPV ^[k]		LUMO [eV] ^[l]	HOMO [eV] ^[m]
		λ_{abs} [nm] ^[h]	λ_{em} [nm] ^[i]	λ_{abs} [nm] ^[h]	λ_{em} [nm] ^[i]	Φ_{F} ^[j]	τ [ns]	E^{red} [V]	E^{ox} [V]		
1a	92 ^[a]	384	499	430	500	0.71	11.1	−1.72	1.22	−3.06	−5.86
1b	80 ^[a]	382	466	374	480	0.82	9.0	−1.61	1.62	−3.16	−6.06
1c	77 ^[a]	475	682	468	670	− ^[n]	− ^[n]	−1.82	0.48	−2.96	−5.07
1d	86 ^[a]	436	589	430	560	0.15	5.5	−1.71	0.94	−3.08	−5.51
1e	91 ^[a]	390	513	370	558	0.56	11.0	−1.73	1.15	−3.06	−5.76
1f	91 ^[a]	389	514	397	510	0.60	9.7	−1.74	1.16	−3.05	−5.75
1g	84 ^[a]	410	554	393	520	0.15	8.4	−1.71	0.96	−3.07	−5.69
1h	81 ^[a]	391	457	390	520	0.05	1.5	−1.47	− ^[n]	−3.29	−6.12
1i	79 ^[a]	384	467	390	480	0.76	8.3	−1.58	− ^[n]	−3.19	−6.02
1j	88 ^[a]	376	457	355	490	0.69	8.2	−1.60	1.60	−3.17	−6.06
1k	81 ^[a]	382	472	355	490	0.76	9.8, 0.9	−1.62	1.59	−3.16	−6.01
1l	66 ^[b]	382	520	355	525	0.42	7.0	−1.74	1.01	−3.04	−5.86
1m	58 ^[a]	423	484	474	670	0.01	− ^[n]	−1.29	− ^[n]	−3.43	−6.15
1n	16 ^[b]	460	635	353	585	− ^[n]	− ^[n]	−1.67	0.76	−3.10	−5.86
2a	77 ^[c]	340	519	350	515	0.04	5.1	−1.80	1.44	−2.98	−5.84
2b	52 ^[d]	337	485	344	475	0.22	9.5	−1.61	1.81	−3.15	−6.18
2c	80 ^[a]	448	596	545	670	0.02	0.86	−1.82	0.66	−2.94	−5.21
2d	66 ^[c]	441	616	421	585	− ^[n]	− ^[n]	−1.73	1.01	−3.05	−5.39
2e	52 ^[c]	344	528	363	510	0.04	1.9	−1.79	1.33	−2.97	−5.78
2f	41 ^[c]	350	525	358	505	0.02	1.9	−1.81	1.38	−2.96	−5.82
2g	22 ^[c]	392	558	321	530	0.04	2.6	−1.79	1.06	−2.98	−5.60
2h	60 ^[d]	330	483	341	450	0.01	1.9	−1.42	− ^[n]	−3.37	−6.33
2i	53 ^[d]	341	485	341	485	0.18	11.7	−1.60	− ^[n]	−3.17	−6.15
2j	54 ^[d]	334	466	330	460	0.58	19.4	−1.65	− ^[n]	−3.12	−6.17
2k	69 ^[d]	358	490	375	485	0.15	6.4, 13.4	−1.66	− ^[n]	−3.09	−6.03
2m	38 ^[c]	391	501	315	450	− ^[n]	1.0, 9.0	−1.31	− ^[n]	−3.45	−6.18
2n	18 ^[c]	466	660	320	380	− ^[n]	− ^[n]	−1.69	0.82	−3.08	−5.32
3a	42 ^[c]	392	579	376	604	0.02	2.7, 1.1	−1.18	1.59	−3.62	−5.81
3b	33 ^[d]	388	544	389	578	0.11	3.6	−1.02	− ^[n]	−3.82	−6.05
3c	53 ^[a]	536	693	563	744	0.02	− ^[n]	−1.31	0.78	−3.46	−5.28
3d	20 ^[c]	493	− ^[n]	500	− ^[n]	− ^[n]	− ^[n]	−1.24	1.13	−3.51	−5.31
4a	92 ^[e]	481	585	487	665	0.02	4.9	−1.03	1.40	−3.78	−5.79
4b	81 ^[f]	471	549	460	640	0.11	4.0	−0.87	− ^[n]	−3.92	−6.01
4c	77 ^[e]	609	− ^[n]	640	− ^[n]	− ^[n]	− ^[n]	−1.13	0.66	−3.63	−5.17
4d	87 ^[e]	− ^[n]	− ^[n]	562	− ^[n]	− ^[n]	− ^[n]	−1.08	1.17	−3.70	−5.37
4e	89 ^[e]	483	609	494	703	0.12	3.6	−1.00	1.33	−3.74	−5.65
4f	85 ^[e]	477	590	496	688	0.19	3.8	−1.05	1.33	−3.70	−5.64
4g	28 ^[e]	484	671	475	764	0.01	0.7, 3.6	−1.04	1.13	−3.70	−5.53
4h	24 ^[e]	446	540	467	632	0.51	3.5, 4.3	−0.84	− ^[n]	−4.00	−6.10
4i	73 ^[e]	451	557	474	658	0.01	3.8, 5.0	−0.87	− ^[n]	−3.93	−5.99
4j	11 ^[e]	451	552	468	630	0.38	5.4, 3.7	−0.88	− ^[n]	−3.91	−6.06
4k	67 ^[e]	471	571	465	663	0.28	3.9	−0.89	1.73	−3.86	−5.94
5a	80 ^[e]	− ^[n]	− ^[n]	541	> 800	− ^[n]	− ^[n]	−0.99	0.84	−3.81	−5.32
5b	11 ^[f]	− ^[n]	− ^[n]	530	780	− ^[n]	− ^[n]	−0.76	1.31	−4.07	−5.68
5c	36 ^[e]	− ^[n]	− ^[n]	648	− ^[n]	− ^[n]	− ^[n]	−1.18	0.34	−3.62	−4.98
5d	6 ^[e]	− ^[n]	− ^[n]	643	− ^[n]	− ^[n]	− ^[n]	−1.09	0.60	−3.73	−5.18
5e	27 ^[e]	− ^[n]	− ^[n]	546	> 800	− ^[n]	− ^[n]	−1.04	0.79	−3.75	−5.26
5f	25 ^[e]	− ^[n]	− ^[n]	551	> 800	− ^[n]	− ^[n]	−1.04	0.72	−3.75	−5.26

[a] 220 °C, 2 h, with catalytic amount of Zn(OAc)₂. [b] 200 °C, 2 h, with 10 equiv of imidazole. [c] 100 °C, 1 h in H₂O, then heated at 300 °C for 1 h. [d] 100 °C, 1 h in H₂O, then heated at 300 °C for 2 h. [e] 250 °C, 3 h, with catalytic amount of Zn(OAc)₂. [f] 300 °C, 3 h, with catalytic amount of Zn(OAc)₂. [g] In CH₂Cl₂. [h] The lowest energy maxima. [i] Excited at the lowest energy maxima. [j] Absolute fluorescence quantum yield determined by a calibrated integrating sphere (errors < 10%). [k] Determined by differential pulse voltammetry in 0.1 M solution of Bu₄NClO₄ in CH₂Cl₂ (1 and 2) or film (3, 4 and 5) (vs. Fc/Fc⁺). [l] Estimated versus vacuum level from $E_{\text{LUMO}} = -4.80 - E_{1/2}^{\text{red}}$, where $E_{1/2}^{\text{red}}$ was determined by cyclic voltammetry in 0.1 M solution of Bu₄NClO₄ in CH₂Cl₂ (1 and 2) or film (3, 4 and 5) (vs. Fc/Fc⁺). [m] Estimated from HOMO=LUMO− E_{g} , where E_{g} was calculated from the onset of absorption spectra (1 and 2: solution, 3–5: film). [n] Not estimated due to low solubility or weak signal.

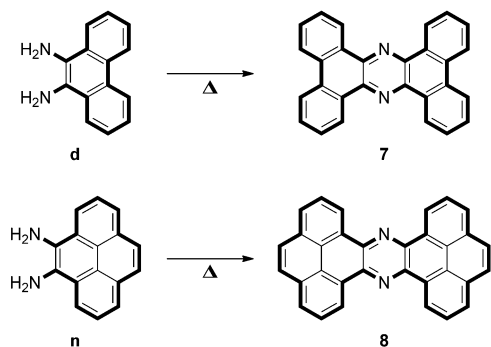
high temperature (280 °C). Di-pyreno[4,5-*b*:4',5'-*e*]pyrazine, **8**, was found as the main product of this reaction, presumably owing to the decomposition of diamine **n** followed by reaction with 4,5-diaminopyrene. To confirm this hypothesis, 9,10-diaminophenanthrene, **d**, or 4,5-diaminopyrene, **n**, were heated alone at 250 °C (Scheme 3). At that temperature, almost all **d** and **n** reacted to form pyrazine products **7** and **8**. The conclusion is that this side reaction prevents the condensations with the carboxylic anhydride in the solid state. Thus, the reaction conditions using imidazole was attempted; although the yields of **1d** and **1n** were improved, the pyrazine side-products were still formed.

The asymmetric diamines **e**–**k** gave two isomers of the products, which were not separated. The ratios of isomers determined by NMR spectroscopy were not 50:50 because the electron-donating/withdrawing properties of the functional groups affect the nucleophilicity of the amino group. The amino groups with an electron-donating methyl or methoxy group at the *o*-position or *p*-position display stronger nucleophilicity compared with the diamines with substituents in *m*-position. Particularly, the *p*-substitution results in rapid formation of the imide unit while the remaining amino group reacts to close the imidazole ring. Thus, the products with electron-donating substituents at the 11-position were obtained in higher yields, which is consistent with the literature.^[13] Similarly, the products with electron-withdrawing groups at the 11-position were obtained in lower yields (Figure 3).

An exception was the 1,2-diamino anthraquinone, **m**, which provided only the product **1m**. This is believed to be caused



Scheme 2. Synthesis of thiophene derivatives.



Scheme 3. Competing side reaction for **d** and **n**.

by steric hindrance between carbonyl and quinone oxygen atoms.

In the reaction of **2** with **a**, the relatively strained fused five-membered rings of the formed BBIs led partly to a disproportionation reaction and the formation of sideproducts **11** and **12** (Scheme 4). As mentioned previously, the reactions to yield **2** and **3** were carried out in water heated to reflux and the formed precipitate was subsequently heated to give BBI and pyrone products (Figure 1). Although these conditions dra-

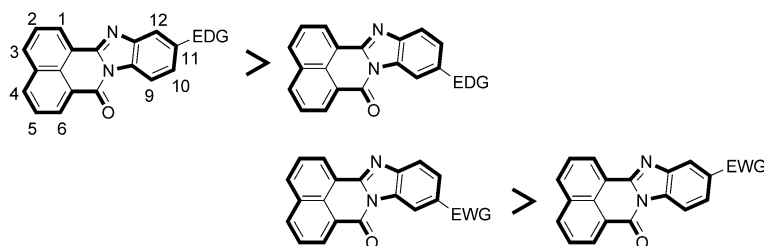
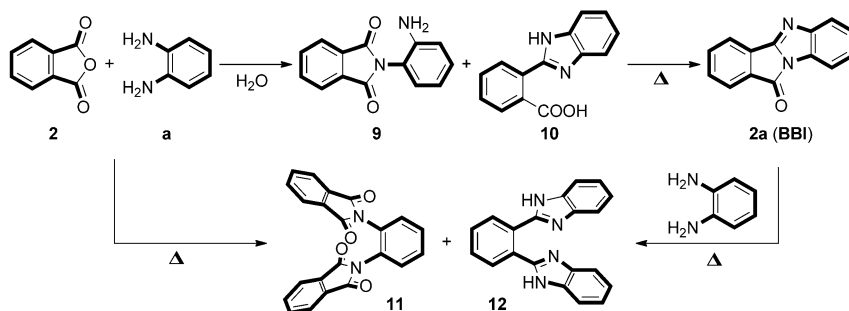


Figure 3. The yield of the isomers differs with the position of the substituent as well as electronic nature of the substituent.



Scheme 4. Competing side reaction for **2a**.

matically decreased the formation of side products **11** and **12**, this reaction could not be completely suppressed. Furthermore, in the case of diamines with electron-donating substituents, the formation of derivatives of **12** might further accelerate owing to the higher nucleophilicity of diamines. For example, the reaction yields of **2e**, **2f**, and especially **2g** were lower than that of **2a**. Conversely, the diamines with electron-withdrawing groups gave lower yield of the side product **12**, presumably owing to the lower nucleophilicity of the diamines. The reaction yields were moderate for those derivatives. The ratio of isomers **2e–2k** displays the same trends as the mixtures of isomers **1e–1k**. The yields of the products and methods used are listed in Table 1.

From the perspective of organic semiconductors, most important are the compounds of the series **4** and **5** (NTCBIs and PTCBIs). Here, the reaction requirements are similar to the NBI **1**, and SSC-DS was successfully employed. However, to prevent incomplete reactions, an excess of diamines (3 mol equivalent for **4** and 4 mol equivalent for **5**) was used. In the reactions between **4** and 4-methoxy-1,2-benzenediamine, **g**, or 4-nitro-1,2-benzenediamine, **h**, the yields were relatively low as the products **4g** and **4h** decomposed during the sublimation (300–400 °C under a vacuum of 10^{-6} Torr). This observation was confirmed by differential scanning calorimetry (DSC) measurements of **4g** and **4h** that showed a broad exothermic peak around 400 °C. Higher vacuum conditions might be required to increase the reaction yields for these compounds. Interestingly, the product **4k** from one of diaminopyridines was obtained in good yield, whereas the product **4j** from 3,4-diaminopyridine, **j**, resulted in low yield. This also might be due to instability of the product **4j** with the stronger electron-accepting properties of 3,4-diaminopyridine, **j**. Unfortunately, the products **4l** and **4n** from 3,4-diaminothiophene and 4,5-diaminopyrene were not obtained, presumably owing to the low stability of the diamines and imide intermediate. In addition, the product **4m** decomposes before evaporating during sublimation owing to high molecular weight.

For the perylene derivatives **5**, with the exception of compound **5a**, only modest yields were obtained owing to the thermal decomposition of the products. The compounds **5g**, **5h**, and **5j**, which correspond to the unstable products in the series **4**, were difficult to purify by sublimation. Here, the product purification would require a significantly higher vacuum level.

Absorption properties

The UV spectra of the compounds from series **1**, **4**, and **5** are shown in Figure 4; the spectra for **2** and **3** are shown in the Supporting Information. In addition, the spectroscopic data are summarized in Table 1. Compared with the parent benzimidazole core obtained from condensation of an anhydride with 1,2-diaminobenzene **a**, the electron-withdrawing groups induced a blueshift, and the substitution of the electron-donating group or a π -extension resulted in a redshift. The compounds with electron-withdrawing groups display high molar extinction coefficients; conversely, the compounds with electron-donating groups display low extinction coefficients. For example, **1h** (NO₂) showed 26000 M⁻¹cm⁻¹ and **11** (Th) showed only 8000 M⁻¹cm⁻¹, compared with 13000 M⁻¹cm⁻¹ of unsubstituted **1a**. Compound **1m**, with the anthraquinone moiety, showed a redshift of absorption maximum with a higher extinction coefficient of 24000 M⁻¹cm⁻¹, most likely owing to the extension of the π -electron system. The UV spectra for series **2** showed similar trends. The exception was pyri-

dine derivative **2k**, which showed redshifted absorption characteristics compared with the parent compound **2a**.

The compounds of series **3** showed a redshift of approximately 50 nm compared with monosubstituted congeners of series **2** in solution, which appears to be due to the extension of the π -electron system.

The compounds of series **4** also showed a redshift compared with the monosubstituted congeners (series **1**). Here, however, the redshift was fairly dramatic, exceeding 80 nm in several examples both in the solution and in the solid state (film). Thus, for example, **4a** was found to be redshifted by 97 nm from **1a**, **4b** by 89 nm from **1b**, etc. The most dramatic shift was observed for **4c**, which was redshifted by 134 nm compared with **1c**.

The compounds of series **5**, the PTCBI series, showed poor solubility and their UV/Vis absorption spectra were recorded in thin film. The films of **5a–5f** showed absorption with an additional 50 nm shift from the compounds of series **4**. Thus, the absorption bands in the region 450–800 nm give these materials a purple to black appearance, a property that could be potentially utilized in organic photovoltaics.

The compounds **5a** and **5b** show similar spectral properties to the methyl-substituted compounds **5e** and **5f**. On the other hand, compounds **5c** and **5d**, derived from 1,8-diaminonaphthalene and 9,10-diaminophenanthrene, showed absorption maxima at 648 and 643 nm, respectively, which is a redshift of approximately 100 nm from PTCBI (**5a**). Thus, the two naphthalene and phenanthrene moieties comprise an extended π -electron system that has a dramatic effect on the HOMO–LUMO gap.

Emission properties

The fluorescence spectra of NBIs (**1a–1n**) are shown in Figure 5 and Table 1; the spectra for compounds **2**, **3**, and **4** are shown in the Supporting Information. The emission maxima show spectral shifts corresponding to their UV/Vis absorption maxima. The Stokes shifts remained substantial across the series, frequently exceeding 100 nm. With agreement to energy-gap law,^[14] the benzimidazole derivatives substituted with electron-donating groups exhibited relatively lower quantum yields. Similarly, low

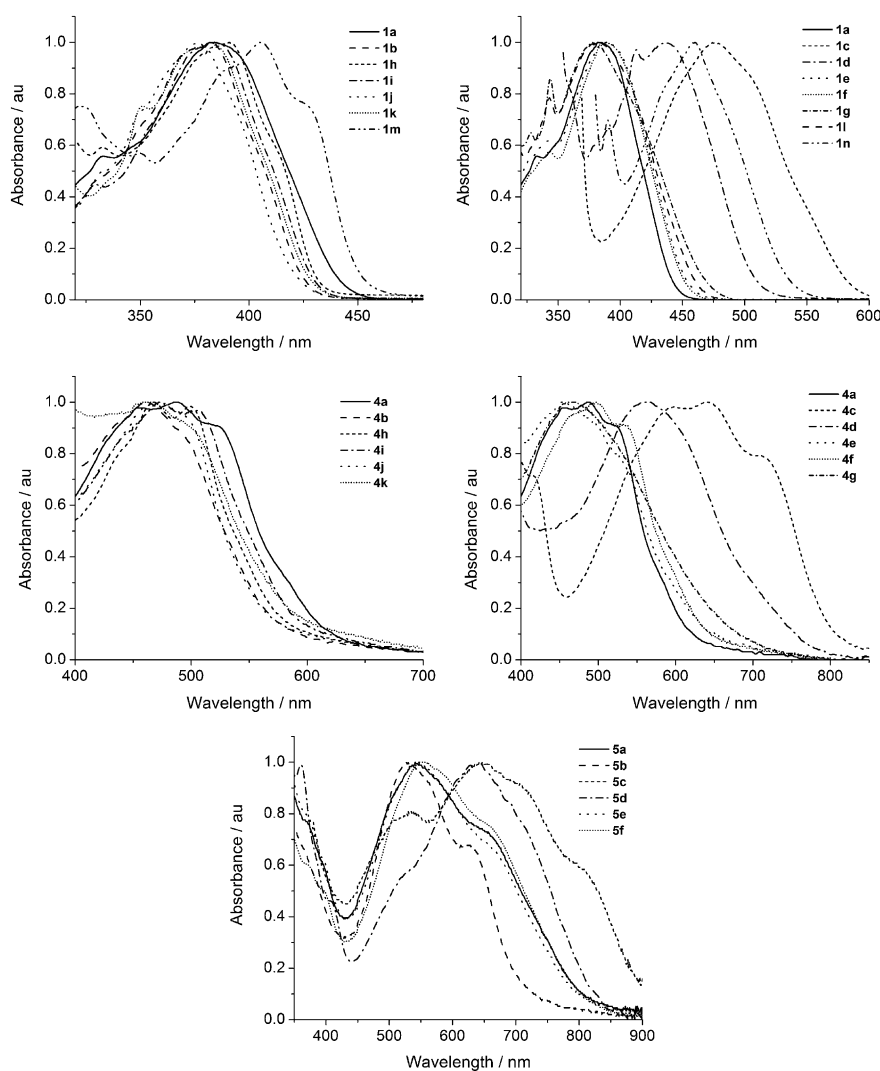


Figure 4. UV/Vis spectra of **1a–1n** in dichloromethane and **4a–4k** and **5a–5f** in thin films.

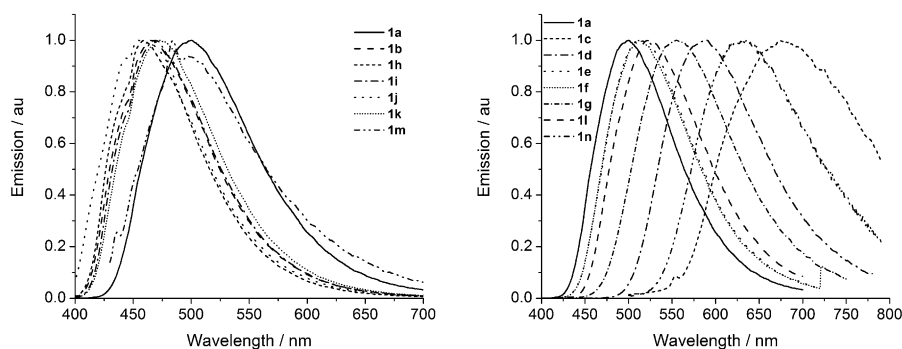


Figure 5. Fluorescence spectra of 1 a–1 n.

fluorescence intensity was also observed for the derivatives with diamine π -moieties such as phenanthrene **1c** and pyrene **1n**. In these two derivatives, the low fluorescence intensity precluded recording fluorescence quantum yields and lifetimes. On the other hand, the naphthoylene benzimidazoles with electron-withdrawing groups, such as perfluorophenyl, pyridyl, or cyano-groups, generally resulted in higher quantum yields (70–80%) and may have potential as blue emitters in organic electronics. The compounds of series **2** showed larger Stokes shifts than those of series **1**, resulted in lower energy emissions, and have weak emissions with less than 5% fluorescence quantum yield. However, some electron-withdrawing groups led to moderate quantum yields.

Electrochemical properties and HOMO–LUMO energies

Cyclic voltammetry (CV) measurements are frequently used to determine the HOMO–LUMO levels of materials from their oxidation and reduction potentials. Thus, the electrochemical properties of products were investigated by CV and differential pulse voltammetry (DPV). Table 1 summarizes the first redox potentials measured by DPV and the corresponding HOMO–LUMO energies. As the structures of the compounds in this study are based on an electron-deficient core, the reduction potentials could be measured for all products. Although some of the compounds also showed oxidation peaks, to enable comparison among the derivatives, the HOMO energies were calculated from the optical energy gap and LUMO levels were estimated from the first reduction potential. The reduction processes were found to be mostly quasi-reversible (Figure 6); however, irreversible oxidation processes were also observed (see the Supporting Information).

When comparing the redox potentials recorded for series **1** and **2**, one can see that series **2** displays larger energy gaps and corresponding redox potentials than series **1**. The effect of substituents was very similar in series **1** and series **2**. The redox potentials are correlated to the electron-withdrawing or electron-donating nature of the functional groups attached to the benzene ring. Thus, compounds with electron-withdrawing groups have small reduction and large oxidation potentials and electron-donating groups have the opposite properties, trends that are described by the inductive effect of functional groups and the stabilization of anion or cation radicals, respec-

tively. The extension of π -conjugation in compounds **1c**, **1d**, and **1n** resulted in lower values of oxidation potentials. These trends in substitutions are similar in series **3–5**. However, in series **3** and **4**, the values of the reduction potentials are much lower and oxidation potentials are a little bit higher compared with those of series **2** and **1**, respectively. Compounds of series **5**

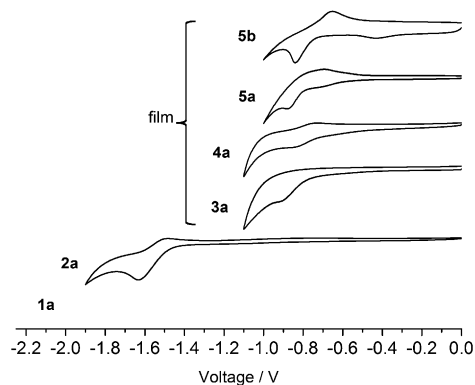


Figure 6. Cyclic voltammetry measurement for **1a** and **2a** in dichloromethane, and **3a**, **4a**, **5a**, and **5b** in thin films (vs. Ag/AgNO₃).

showed two reduction peaks. The first reduction potentials of series **5** were only slightly shifted to the positive side from those of series **4**. Therefore, the electron-accepting properties in series **4** and **5** should be similar despite larger π -conjugation in perylene derivatives, **5**. The oxidation potentials in series **5** were lower compared with series **4**.

Figure 7 summarizes the experimental and theoretical HOMO–LUMO levels of products **1a–5a** and related materials, and shows the effect of the structural features on the HOMO–LUMO levels.^[15] Thus, **1a** (NBI) has a slightly smaller gap than **2a** (BBI) owing to a larger conjugation length in **2a**. **3a** (pyrro) and **4a** (NTCBI) show a similar trend. The extension of π -conjugation by an additional benzimidazole site from **1a** to **3a** or **2a** to **4a**, significantly lowers the LUMO levels while showing only a small upward shift in the HOMO levels.

These trends are in agreement with the trends revealed by DFT calculations (B3LYP/6-31+G(d,p) level). The extension of the π -core in **5a** (PTCBI) compared with **4a** affected the LUMO level less, but resulted in the HOMO level shifting to a higher level.

The HOMO–LUMO energy levels of organic semiconductors are a crucial and necessary factor for the design of multilayer devices. However, their values depend on the method of estimation. The HOMO–LUMO level of PTCBI has been investigated owing to its application in organic photovoltaics. The HOMO level is expected to be -6.2 eV from ultraviolet photoelectron spectroscopy (UPS).^[16] The LUMO level of PTCBI is esti-

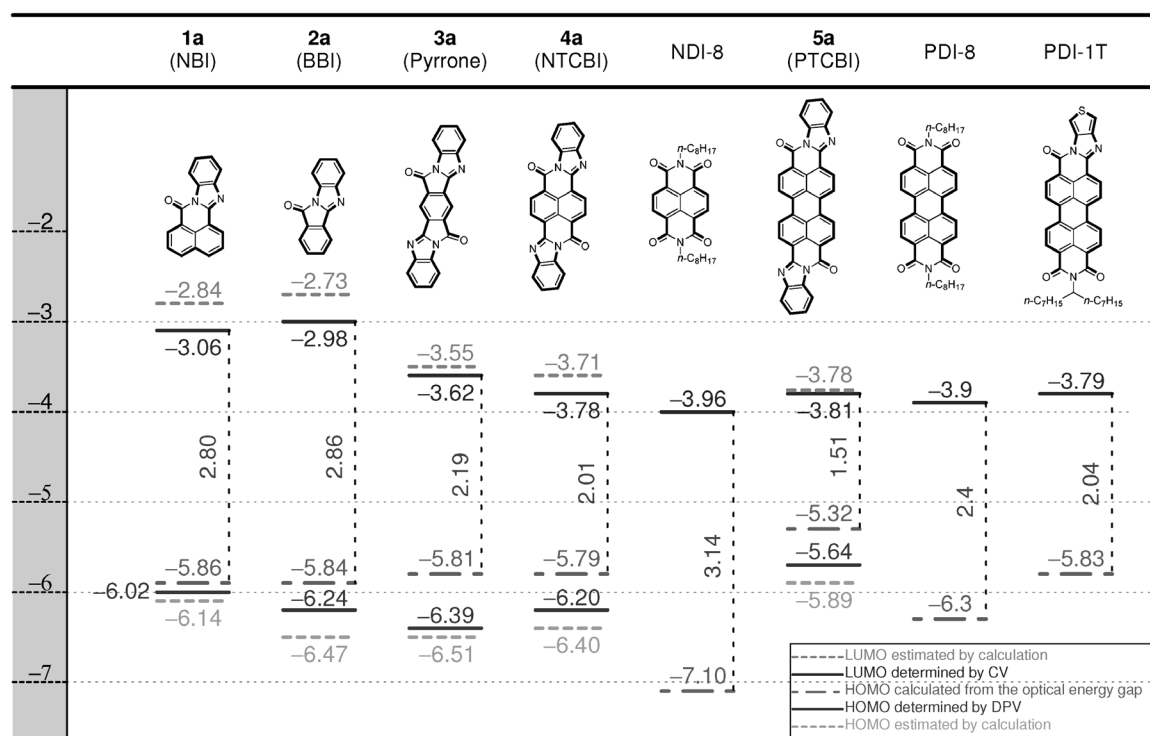


Figure 7. The HOMO–LUMO energy diagrams of **1a–5a** and related materials.

mated from optical energy gap to be -4.5 eV. These values are significantly different from the DFT calculations and our estimation using electrochemical measurements in film (Figure 7). The LUMO level of PTCBI determined from electrochemical measurements in film was -3.78 eV, which is consistent with the DFT calculation. In addition, the related materials, NDI-8, PDI-8, and PDI-1T, have similar LUMO energies, suggesting the accurate estimation of the LUMO level for PTCBI. The LUMO energy of -4.5 eV in literature is not a directly observed value, but one calculated from the HOMO–LUMO gap measured by absorption spectroscopy. In fact, inverse photoelectron spectroscopy (IPES) for PTCBI revealed the LUMO energy to be -4.0 eV,^[17] which is close to our result. Our estimation of the HOMO level is -5.64 eV, which is also different from the result from UPS. Importantly, the HOMO–LUMO levels from UPS and IPES or even from redox potentials give large energy gaps compared with the estimation from optical measurement. This suggests that the absorption spectra are significantly affected by aggregation of the large π -conjugated molecules, a fact that generally leads to redshifted onset resulting in unrealistically low estimates for the HOMO–LUMO gap.

Crystal structures

Crystal structure analysis is important for organic semiconductors because the molecular arrangement and intermolecular interactions significantly affect the charge-transport behavior. Single crystals suitable for X-ray structure analysis were grown by slow sublimation for some of the products. The molecules have almost planar structures and the packing motif displayed sig-

nificant π – π stacking (Figure 8). For compound **3b**, only the *cis*-isomer was grown as a crystal of a good quality. Unfortunately, crystals of the *trans*-isomer of **3b** could not be obtained thus far. Compound **1m** showed only one geometry, which is in agreement with the NMR spectra. The interatomic N...H and O...H contacts with adjacent molecules were observed along the *bc* plane. On the other hand, short atomic contacts were not observed in the direction of the π – π stacking, resulting in a relatively weak intermolecular interaction with the distance of 3.39 Å between the molecular planes. As seen in the crystal of **1b** in the previous report,^[11] the fluorinated compounds **2b** and **3b-cis** showed strong intermolecular interactions with a number of three-dimensional interatomic short contacts. Those molecules display O...H–C and F...H–C interactions within 2D sheets. The structure of **3b-cis** displays a rarely observed F...F interaction of type II^[18] with the distance of 2.82 Å. Although those short contacts are relatively weak interactions, they caused the formation of dense π -conjugation sheets. The packing coefficients calculated by PLATON/VOID software were 74.5% for **1b**, 74.4% for **2b**, and 74.0% for **3b-cis**.^[19] Molecule **2b** displays a large dipole moment of 5.9 Debye calculated at the B3LYP/6-31+G(d,p) level; the dipole moments are aligned in the same direction in the 2D sheets. Conversely, the molecular sheets were aligned in the opposite direction, so the dipole moments are canceled out by interlayer interactions. The π – π stacking of **2b** included C...C contacts of approximately 3.3 Å and a C...F contact of 3.13 Å. In addition, **3b-cis** has strong intermolecular interactions along the π -stacking direction with C...C contacts of approximately 3.3 Å and other contacts such as C...N, C...O, C...F, and N...F. **3b-cis** displays a small dipole

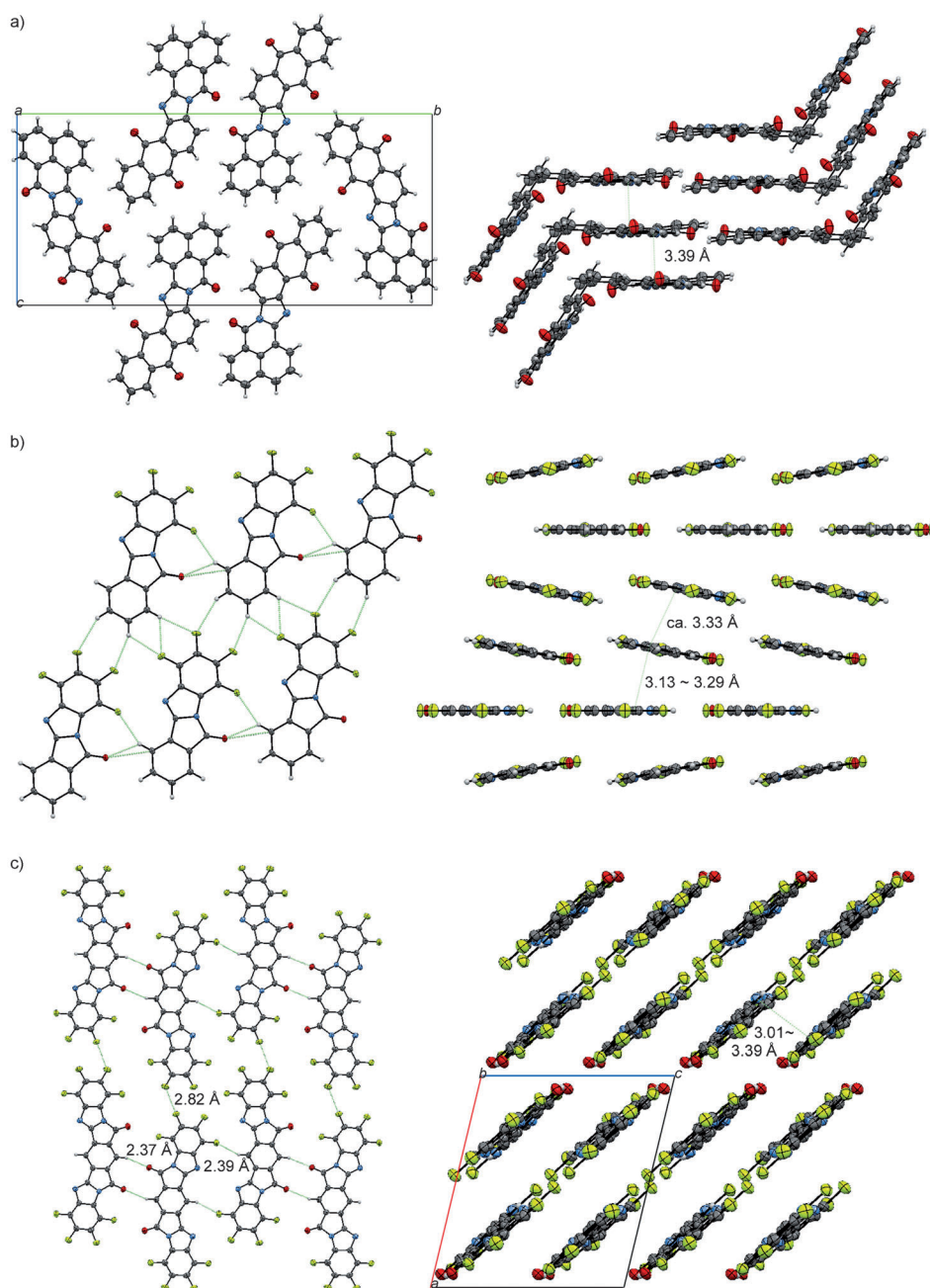


Figure 8. Crystal structures of (a) **1m**, (b) **2b**, and (c) **3b** (*cis*-isomer) (thermal ellipsoids set at 50% probability).

moment of 0.23 Debye. It appears to be clear that the fluoro-substitution has a great influence on the crystal structure and is a basis for strong intermolecular interactions.

Semiconductor film morphology

The interfaces between the source/drain electrodes and semiconductor are important for the charge transport. Thus, film morphology as observed by AFM is important in field-effect transistor devices with the top-contact configuration. Although the dielectric semiconductor interface, which is the other important region for charge transport, cannot be probed, the

film morphology and the growth of grains usually correlate with the charge transport.^[20]

Film morphology of the evaporated films of **3a**, **3b**, **4a**, and **4b** on hexamethyldisilazane (HMDS)-treated substrate was studied by using tapping-mode atomic-force microscopy (AFM; Figure 9). The film of **3a** showed large crystalline plates growing in perpendicular directions to the surface. As a result, large differences in height were observed. Such surfaces may prevent formation of electrodes on the top. On the other hand, the films of **3b**, **4a**, and **4b** showed relatively small grains in the films. The film of **4b** shows the flattest surface and grains seem to be connected to each other. Such a microstructure reduces grain boundary and facilitates charge transport.

Field-effect transistor characteristics

The FET devices were fabricated with top-contact configuration with Au electrodes. The SiO₂ gate dielectric layer was treated with HMDS, poly(methyl methacrylate) (PMMA), polystyrene, Teflon, or CYTOP™ (a fluorinated polyether) as the organic gate dielectric layer. The devices with PMMA and Teflon showed slightly lower performances than others. The FET characteristics are summarized in Table 2. The devices showed typical n-type semiconducting behavior. The

exception was compound **3a**, where the lack of semiconductor behavior is attributed to the film morphology shown in Figure 9. Although the LUMO levels of **3b** and **4a** are similar, the mobilities in **4a** are one order of a magnitude lower. Further, from the materials tested, the compounds **3b** and to a lesser extent **4b** showed the best performance in the experimental OFETs.

The films of **3b** and **4b**, having a lower LUMO levels, showed almost the same mobilities, with values of 0.03 and 0.01 cm²V⁻¹s⁻¹, respectively. This confirms our hypothesis that the fluorine substitution aids in achieving high electron mobility. However, the differences in LUMO levels owing to the core structures, affect the turn-on and threshold voltages. Thus, in

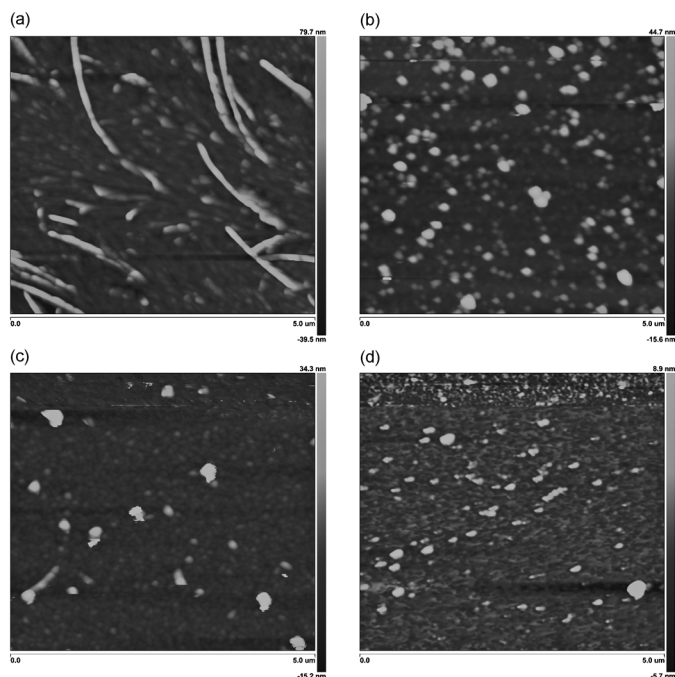


Figure 9. AFM images of vapor-deposited films of (a) **3a**, (b) **3b**, (c) **4a**, and (d) **4b** grown at room temperature on HMDS-treated substrate.

Table 2. Field-effect transistor characteristics. ^[a]				
Compound	Surface treatment	Mobility [cm ² V ⁻¹ s ⁻¹]	On/off ratio	Threshold [V]
3b	polystyrene ^[b]	0.027	3 × 10 ³	26
	HMDS	0.019	5 × 10 ³	20
	CYTOP ^[b]	0.01	1 × 10 ³	29
4a	polystyrene ^[b]	5 × 10 ⁻³	1 × 10 ³	8
	HMDS	9 × 10 ⁻⁴	1 × 10 ²	23
	CYTOP ^[b]	3 × 10 ⁻³	1 × 10 ²	8
4b	polystyrene ^[b]	0.013	2 × 10 ³	18
	HMDS	0.013	1 × 10 ³	12
	CYTOP ^[b]	7 × 10 ⁻³	2 × 10 ³	20

[a] SiO₂: 200 nm, active layer: 50 nm, L/W = 75 μm/1000 μm, S/D electrode: 50 nm Au. [b] Thickness: ca. 20 nm.

the transfer curves for the film of **4b** (Figure 10, circles), the current started to increase from almost 0 V, suggesting a good electron injection, whereas the rising edge of current for **3b** is somewhat shifted to higher potentials (squares; Figure 10).

The devices fabricated by using polystyrene for **3b** and **4b** showed higher mobilities than HMDS-treated devices, although the threshold voltages were also higher. The same trends were observed for a semiconductor with a similar LUMO level.^[21] This is attributed to the effective passivation of surface chemical defects, reduction of trap density on polystyrene, and the relatively small dielectric constant of polystyrene. The devices with **3b** and **4b** deposited on a polystyrene substrate showed mobilities of 0.027 cm²V⁻¹s⁻¹ and 0.013 cm²V⁻¹s⁻¹, and threshold voltages of 26 V and 18 V, respectively.

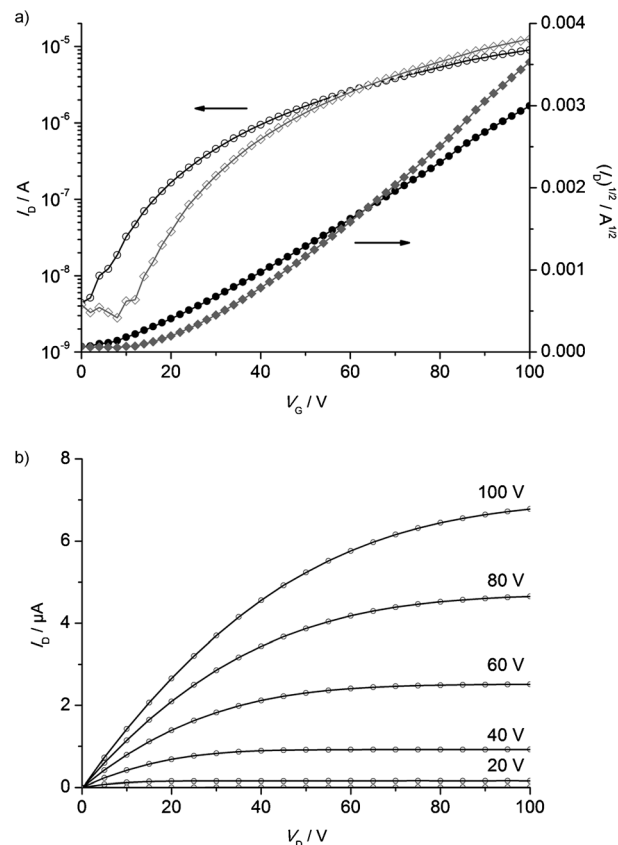


Figure 10. (a) Drain–source current (I_D) and $(I_D)^{1/2}$ versus gate voltage (V_G) at drain voltage of 100 V transfer characteristics for the device deposited on polystyrene; squares (gray lines) are the device for **3b** and circles (black lines) are the device for **4b**. (b) I_D versus drain–source voltage (V_D) output characteristics for **4b**.

The film of **4a** displayed only moderate mobility (0.005 cm²V⁻¹s⁻¹), whereas the corresponding polymer, BBL, synthesized from tetraaminobenzene showed a high mobility of 0.05 cm²V⁻¹s⁻¹.^[22] This is attributed to the difference of molecular orientations and π -electron delocalization. In the NTCBI series of compounds (series **4**) the electron transport does not seem to be effective unless an electron-accepting moiety is placed at the terminal position such as the multiple fluoro-substituents in **4b**. It is important to note that these results are based on the mixture of *cis*-/*trans*-isomers. Some literature reports have pointed out that the mixture of isomers decreases the field-effect mobility.^[23] Thus, the isomerically pure compounds might show higher OFET device performances.

Conclusion

We have synthesized a series of benzimidazoles of carboxylic acids by a green route based on solid-state condensation and direct sublimation (SSC-DS), a method that utilizes solvent-free reaction conditions and purification. Most of the compound of series **1** and **2** were obtained in good yields except the compounds comprising thiophene and pyrene, where the diminished yields are due to the instability of the starting diamines. In the PTCBI series, **5**, the substituents decreased the reaction

yields and some products could not be isolated owing to the high sublimation temperature used for purification. As expected, the electronic nature of the substituents enabled tuning of the UV/Vis absorption and emission maxima. In several instances, the limited solubility of the benzimidazole products led to aggregation and corresponding redshifted absorption spectra. Such spectra, when used to calculate HOMO–LUMO energy gap, may provide unrealistic values of the energy levels, particularly in the cases where the oxidation peaks are not directly accessible. In all the series of compounds discussed herein, the absorption and emission energies tend to correlate with the extinction coefficient and the quantum efficiency. Cyclic voltammetry and differential pulse voltammetry displayed quasi-reversible reductions for the studied compounds, suggesting n-type behavior. This has been confirmed in experimental field-effect transistors, where use of these materials showed n-type transistor characteristics with the mobilities of $\sim 10^{-2} \text{ cm}^2 \text{ V}^{-1} \text{ s}^{-1}$. Importantly, it was found that compounds comprising fluorinated fragments derived from 1,2-diamino-3,4,5,6-tetrafluoro-benzene showed the ability to form a large number of C...F and N...F intermolecular interactions and short contacts, contributing to the formation of small grains in the films. We presume that these features enabled the relatively high electron mobilities ($\sim 0.03 \text{ cm}^2 \text{ V}^{-1} \text{ s}^{-1}$). This finding will be explored in following studies as we believe that it will enable the design of novel n-type semiconductors for OFET applications.

Experimental Section

Instruments

Mass spectra were collected on a Shimadzu Gas Chromatography–Mass Spectrometry (GC–MS) QP5050 A instrument equipped with a direct probe ionization. MALDI–TOF/MS spectra were recorded by using a Bruker Daltonics Omnisflex spectrometer. FD–TOF/HRMS spectra were obtained on a JEOL JMS–T100GC. ^1H NMR and ^{13}C NMR spectra were recorded on a Bruker DRX–300 (300 MHz) or 500 MHz Bruker instrument. Chemical shifts were calibrated to the corresponding deuterated solvents. Melting points were obtained on a Shimadzu DSC–60. The UV/Vis spectra were measured by using a HP (Hewlett Packard) single-beam spectrophotometer with a diode array or a Hitachi U–3010 double-beam spectrophotometer, accurate to $\pm 0.3 \text{ nm}$. The light source consisted of Deuterium (D2) and Tungsten Iodide (50W) lamps for the ultraviolet and visible regions, respectively. The concentration of the solutions was adjusted so that the measured absorbances would range between 0.1 and 0.3 for the optical measurements. Emission spectra were recorded by using a spectrofluorimeter from Edinburgh Analytical Instruments (FL/FS 900). Compounds were dissolved in freshly distilled dichloromethane prior to measurements. The fluorescence quantum yields of the luminophores were measured by absolute measurement of the photoluminescence quantum yield (APLQY) using an integrating sphere (Sphere Optics 70°) and an Andor CCD camera (DU401–FI), the spectral flux was calibrated by using a halogen lamp (Sphere optics LCS–100–5W, serial number 3999). The excitation sources were a 375 nm laser diode (PicoQuant, LDH–D–C–375B) and a 355 nm laser diode (Crystal Laser, QC 355–050), the method was modified from previous reports.^[24] The steady-state lifetime measurements were recorded in a time-correlated single-

photon-counting spectrofluorimeter from Edinburgh Analytical Instruments (FL/FS 900) with a photomultiplier tube in a Peltier-cooled housing. The excitation sources used were the same 375 nm laser diode from PicoQuant (LDH–D–C–375B) and the 355 nm laser diode from Crystal Laser (QC 355–050). The lifetimes of the samples that needed blue light as the excitation source were measured in a LifeSpec II time-correlated single-photon-counting spectrometer from Edinburgh Instruments, the excitation source used was a Ti:Sapphire laser (Chameleon Ultra II, Coherent), the pulses were picked at 4 MHz for the repetition rate, and the excitation wavelengths were selected between 440 nm and 480 nm by a frequency-doubling unit (APE–GmbH SHG). Cyclic voltammetry (CV) and differential pulse voltammetry (DPV) were carried out on a CH instruments Electrochemical Workstation CHI430. Tetrabutylammonium perchlorate (TBAP; 0.1 M) in argon-purged CH_2Cl_2 was used as the supporting electrolyte at room temperature. The conventional three-electrode configuration consisted of a platinum or an indium tin oxide (ITO) working electrode, a platinum wire auxiliary electrode, and an Ag/AgNO₃ reference electrode. Each measurement was calibrated using ferrocene/ferrocenium (Fc/Fc^+) as a standard. Cyclic voltammograms were obtained at a scan rate of 100 mV s^{-1} . The elemental analysis was performed with a PerkinElmer 2400 Series II CHNS/O system (Waltham, MA) equipped with PerkinElmer EA Data Manager software. The purification was carried out in a three-zone sublimation apparatus (Lindberg/Blue Thermo Electron Corporation). X-ray diffraction data were collected on a Nonius Kappa CCD diffractometer, Rigaku SCX–Mini with Mercury CCD diffractometer, and Rigaku AFC–12 with Saturn 724+ CCD diffractometer with $\text{Mo}_{\text{K}\alpha}$ radiation ($\lambda = 0.71075 \text{ \AA}$). Single crystals suitable for X-ray analysis were grown by slow sublimation.

General procedures for the syntheses

3,4-Diaminothiophene **1** was synthesized according to reported methods^[25] and 4,5-diaminopyrene **n** was synthesized in three steps from pyrene, with a total yield of 20%, by the modification of the reported procedure for 9,10-diaminophenanthrene **d**.^[26]

Procedure 1—solid-state condensation catalyzed by zinc acetate and direct sublimation (SSC–DS): A carboxylic acid anhydride and a diamine were mixed well by using a mortar and pestle. A catalytic amount of zinc acetate (less than 0.1 molar equiv) was added to the mixture. They were stirred and heated to a certain temperature (220–300 °C depending on the combination of anhydride and diamine). After 2–3 h, the reaction mixture was allowed to cool to room temperature. The crude material was sublimed under vacuum (10^{-6} – 10^{-7} Torr), without any other purification, to give the pure compound.

Procedure 2—aqueous condensation and direct sublimation: A carboxylic acid anhydride and a diamine in H_2O were stirred at 100 °C for 2 h. The precipitate was filtered or the reaction solution was evaporated to dryness. The solid was collected and moved to a tube for sublimation. The solid was heated at 300 °C for 1 h under ambient pressure, then sublimed under vacuum (10^{-6} – 10^{-7} Torr).

Procedure 3—with imidazole: A carboxylic acid anhydride, a diamine, and 10 equivalents of imidazole were stirred at 200 °C for 3 h. The reaction mixture was washed with water and dried. The crude material was sublimed under vacuum (10^{-6} – 10^{-7} Torr) without any other purification.

Device fabrication: The HMDS (hexamethyldisilazane) treatment was carried out by immersing the substrate in HMDS at room temperature for >10 h. The Teflon, CYTOP, polystyrene, or PMMA layers (ca. 20 nm) were prepared by spin-coating at 4000 rpm from

1 wt%, 1.5 wt%, 0.5 wt%, and 1 wt% solution, respectively. OFETs were constructed on heavily doped n-type silicon wafers covered with thermally grown silicon dioxide (200 nm), which was cleaned by piranha solution. The silicon dioxide acts as a gate dielectric layer, and the silicon wafer serves as a gate electrode. Organic semiconductors (50 nm) were deposited on the silicon dioxide by vacuum evaporation at a rate of $0.2\text{--}0.3 \text{ \AA s}^{-1}$ under a pressure of 10^{-5} Pa. During the evaporation, the temperature of the substrate was maintained at room temperature. Gold was used as the source and drain electrodes (50 nm) and deposited on the organic semiconductor layer through a shadow mask with $L/W=75/1000 \text{ \mu m}$. The FET measurements were carried out at room temperature in a glovebox without exposure to air with a semiconductor parameter analyzer (4200-SCS, Keithley). The FET performances were not observed under air. Mobilities (μ) were calculated in the saturation regime by the relationship: $\mu_{\text{sat}} = (2I_{\text{D}}L)/[WC_{\text{ox}}(V_{\text{G}} - V_{\text{th}})^2]$, where I_{D} is the source-drain saturation current, C_{ox} (4 F) is the oxide capacitance, V_{G} is the gate voltage, and V_{th} is the threshold voltage. The latter can be estimated as the intercept of the linear section of the plot of $V_{\text{G}} (I_{\text{D}})^{1/2}$.

DFT calculations

All computations were performed with Gaussian 03^[27] using B3LYP/6-31+G(d,p)//B3LYP/6-31G(d,p).

Full experimental details and characterization data are described in the Supporting Information.

Acknowledgements

Support from the AFOSR (Grant No. FA9550-05-1-0276 for P.A.), the State of Ohio (WCI-PVIC), NSF (Grant No. DMR-1006761 for, EXP-LA 0731153, CHE0750303 for P.A.), Japan Regional Innovation Strategy Program by the Excellence (creating international research hub for advanced organic electronics) of Japan Science and Technology Agency (JST), the Ministry of Education, Culture, Sports, Science and Technology, Japan, the UBE foundation, and BGSU is gratefully acknowledged. NSF CRIF Grant No. 0741973 (University of Texas at Austin) was used to purchase the X-ray diffractometer.

Keywords: dyes/pigments · green chemistry · heterocycles · organic field-effect transistors · semiconductors

- [1] M. Herbst, K. Hunger, *Industrial Organic Pigments*, 3rd Ed. Wiley-VCH, Weinheim, 1993.
- [2] a) L. Feiler, H. Langhals, K. Polborn, *Liebigs Ann.* **1995**, 1229–1244; b) M. Adachi, Y. Nagao, *Chem. Mater.* **1999**, *11*, 2107–2114; c) H. Langhals, P. Blanke, *Dyes Pigment.* **2003**, *59*, 109–116; d) M. P. O'Neil, M. P. Niemczyk, W. A. Svec, D. Gosztola, G. L. Gaines, M. R. Wasielewski, *Science* **1992**, *257*, 63–65; e) W. B. Davis, W. A. Svec, M. A. Ratner, M. R. Wasielewski, *Nature* **1998**, *396*, 60–63; f) X. Guo, D. Zhang, D. Zhu, *Adv. Mater.* **2004**, *16*, 125–130; g) R. T. Hayes, M. R. Wasielewski, D. Gosztola, *J. Am. Chem. Soc.* **2000**, *122*, 5563–5567; h) M. Sadrai, L. Hadel, R. R. Sauer, S. Husain, K. Krogh-Jespersen, J. D. Westbrook, G. R. Bird, *J. Phys. Chem.* **1992**, *96*, 7988–7996; i) R. Gvishi, R. Reisfeld, Z. Brushtein, *Chem. Phys. Lett.* **1993**, *213*, 338–344; j) M. J. Ahrens, M. J. Fuller, M. R. Wasielewski, *Chem. Mater.* **2003**, *15*, 2684–2686.
- [3] a) B. A. Jones, M. J. Ahrens, M.-H. Yoon, A. Facchetti, T. J. Marks, M. R. Wasielewski, *Angew. Chem.* **2004**, *116*, 6523–6526; *Angew. Chem. Int. Ed.* **2004**, *43*, 6363–6366; b) R. Schmidt, M. M. Ling, J. H. Oh, M. Winkler, M. Könemann, Z. Bao, F. Würthner, *Adv. Mater.* **2007**, *19*, 3692–3695; c) B. J. Jung, N. J. Tremblay, M.-L. Yeh, H. E. Katz, *Chem. Mater.* **2011**, *23*, 568–582; d) X. W. Zhan, A. Facchetti, S. Barlow, T. J. Marks, M. A. Ratner, M. R. Wasielewski, S. R. Marder, *Adv. Mater.* **2011**, *23*, 268–284; e) C. Wang, H. Dong, W. Hu, Y. Liu, D. Zhu, *Chem. Rev.* **2012**, *112*, 2208.
- [4] a) L. Schmidt-Mende, A. Fechtenkotter, K. Müllen, E. Moons, R. H. Friend, J. D. MacKenzie, *Science* **2001**, *293*, 1119–1122; b) X. Zhan, Z. A. Tan, B. Domercq, Z. An, X. Zhang, S. Barlow, Y. Li, D. Zhu, B. Kippelen, S. R. Marder, *J. Am. Chem. Soc.* **2007**, *129*, 7246–7247; c) J. E. Anthony, *Chem. Mater.* **2011**, *23*, 583–590.
- [5] C. W. Tang, *Appl. Phys. Lett.* **1986**, *48*, 183–185.
- [6] a) J. Xue, S. Uchida, B. P. Rand, S. R. Forrest, *Appl. Phys. Lett.* **2004**, *85*, 5757–5759; b) V. P. Singh, R. S. Singh, B. Parthasarathy, A. Aguilera, J. Anthony, M. Payne, *Appl. Phys. Lett.* **2005**, *86*, 082106; c) P. Dhagat, H. M. Haverinen, R. J. Kline, Y. Jung, D. A. Fischer, D. M. DeLongchamp, G. E. Jabbour, *Adv. Funct. Mater.* **2009**, *19*, 2365–2372; d) B. E. Lassiter, G. Wei, S. Wang, J. D. Zimmerman, V. V. Diev, M. E. Thompson, S. R. Forrest, *Appl. Phys. Lett.* **2011**, *98*, 243307; e) L. Perrin, P. Hudhomme, *Eur. J. Org. Chem.* **2011**, 5427–5440; f) K. Hirao, Y. Tsukada, S. Suzuki, H. Takahashi, J. Mizuguchi, *J. Appl. Phys.* **2008**, *103*, 053706.
- [7] a) A. Babel, S. A. Jenekhe, *Adv. Mater.* **2002**, *14*, 371–374; b) S. Erten, S. Icli, *Inorg. Chim. Acta* **2008**, *361*, 595–600; c) C. Tozlu, S. E. -Ela, S. Icli, *Sens. Actuators A* **2010**, *161*, 46–52.
- [8] a) H. E. Katz, A. J. Lovinger, J. Johnson, C. Kloc, T. Siegrist, W. Li, Y.-Y. Lin, A. Dodabalapur, *Nature* **2000**, *404*, 478–481; b) H. E. Katz, J. Johnson, A. J. Lovinger, W. Li, *J. Am. Chem. Soc.* **2000**, *122*, 7787–7792; c) B. A. Jones, A. Facchetti, T. J. Marks, M. R. Wasielewski, *Chem. Mater.* **2007**, *19*, 2703–2705; d) H. Krüger, S. Janietz, D. Sainova, D. Dobrev, N. Koch, A. Vollmer, *Adv. Mater.* **2007**, *19*, 3715–3723; e) K. C. See, C. Landis, A. Sarjeant, H. E. Katz, *Chem. Mater.* **2008**, *20*, 3609–3616; f) H. Yan, Z. Chen, Y. Zheng, C. Newman, J. R. Quinn, F. Dötz, M. Kastler, A. Facchetti, *Nature* **2009**, *457*, 679–686; g) F. S. Kim, X. Guo, M. D. Watson, S. A. Jenekhe, *Adv. Mater.* **2010**, *22*, 478–482.
- [9] a) R. Blanco, R. Gómez, C. Seoane, J. L. Segura, E. Mena-Osteritz, P. Bäuerle, *Org. Lett.* **2007**, *9*, 2171–2174; b) S. R. González, J. Casado, J. T. L. Navarrete, R. Blanco, J. L. Segura, *J. Phys. Chem. A* **2008**, *112*, 6732–6740; c) R. P. Ortiz, H. Herrera, R. Blanco, H. Huang, A. Facchetti, T. J. Marks, Y. Zheng, J. L. Segura, *J. Am. Chem. Soc.* **2010**, *132*, 8440–8452; d) A. Wicklein, P. Kohn, L. Ghazaryan, T. Thurn-Albrecht, M. Thelak, *Chem. Commun.* **2010**, 46, 2328–2330; e) R. P. Ortiz, H. Herrera, C. Seoane, J. L. Segura, A. Facchetti, T. J. Marks, *Chem. Eur. J.* **2012**, *18*, 532–543; f) Y. Zhang, D. Hanifi, S. Alvarez, F. Antonio, A. Pun, L. M. Klivansky, A. Hexemer, B. Ma, Y. Liu, *Org. Lett.* **2011**, *13*, 6528–6531; g) D. Hanifi, D. Cao, L. M. Klivansky, Y. Liu, *Chem. Commun.* **2011**, 47, 3454–3456.
- [10] a) B. M. Krasovitskii, B. M. Bolotin, *Organic Luminescent Materials*, VCH Verlagsgesellschaft GmbH, Weinheim, 1988; b) N. Z. Galunov, B. M. Krasovitskii, O. N. Lyubenko, I. G. Yermolenko, L. D. Patsenker, A. O. Doroshenko, *J. Lumin.* **2003**, *102–103*, 119–124; c) W. X. Ren, S. Bhuniya, J. F. Zhang, Y. H. Lee, S. J. Lee, J. S. Kim, *Tetrahedron Lett.* **2010**, *51*, 5784–5786.
- [11] M. Mamada, C. Pérez-Bolívar, P. Anzenbacher, *Org. Lett.* **2011**, *13*, 4882–4885.
- [12] J. Mizuguchi, N. Shimo, *J. Imaging Sci. Technol.* **2006**, *50*, 115–121.
- [13] a) L. Lu, L. He, *J. Mol. Struct.* **2012**, *1026*, 1–7; b) D. Singh, J. B. Baruah, *Tetrahedron Lett.* **2008**, *49*, 4374.
- [14] a) J. V. Caspar, T. J. Meyer, *Inorg. Chem.* **1983**, *22*, 2444–2453; b) R. Pohl, P. Anzenbacher Jr., *Org. Lett.* **2003**, *5*, 2769–2772; c) R. Pohl, V. A. Montes, J. Shinar, P. Anzenbacher Jr., *J. Org. Chem.* **2004**, *69*, 1723–1725.
- [15] a) E. A. B. Kantchev, H. S. Tan, T. B. Norsten, M. B. Sullivan, *Org. Lett.* **2011**, *13*, 5432; b) B. A. Jones, A. Facchetti, M. R. Wasielewski, T. J. Marks, *J. Am. Chem. Soc.* **2007**, *129*, 15259; c) M. Luo, Q. Wang, Z. Y. Wang, *Org. Lett.* **2011**, *13*, 4092–4095.
- [16] a) I. G. Hill, J. Schwartz, A. Kahn, *Org. Electron.* **2000**, *1*, 5–13; b) A. Yakimov, S. R. Forrest, *Appl. Phys. Lett.* **2002**, *80*, 1667–1669; c) S. R. Yost, L.-P. Wang, T. V. Voorhis, *J. Phys. Chem. C* **2011**, *115*, 14431–14436.
- [17] A. Kahn, N. Koch, W. Gao, *J. Polym. Sci. B Polymer Phys.* **2003**, *41*, 2529–2548.
- [18] a) N. Ramasubbu, R. Parthasarathy, P. Murray-Rust, *J. Am. Chem. Soc.* **1986**, *108*, 4308–4314; b) K. Reichenbacher, H. I. Süß, J. Hulliger, *Chem. Soc. Rev.* **2005**, *34*, 22–30.

- [19] a) A. L. Spek, *J. Appl. Crystallogr.* **2003**, *36*, 7–13; b) P. Vishweshwar, A. Nangia, V. M. Lynch, *Cryst. Growth Des.* **2003**, *3*, 783–790.
- [20] a) P. Kim, X. H. Zhang, B. Domercq, S. C. Jones, P. J. Hotchkiss, S. R. Marder, B. Kippelen, J. W. Perry, *Appl. Phys. Lett.* **2008**, *93*, 013302; b) T. S. Huang, Y. K. Su, P. C. Wang, *Appl. Phys. Lett.* **2007**, *91*, 092116; c) S. Pyo, H. Son, K. Y. Choi, M. H. Yi, S. K. Hong, *Appl. Phys. Lett.* **2005**, *86*, 133508; d) J. Lee, J. H. Kim, S. Im, *J. Appl. Phys.* **2004**, *95*, 3733–3736; e) S. Y. Park, M. Park, H. H. Lee, *Appl. Phys. Lett.* **2004**, *85*, 2283–2285.
- [21] M.-H. Yoon, C. Kim, A. Facchetti, T. J. Marks, *J. Am. Chem. Soc.* **2006**, *128*, 12851–12869.
- [22] A. Babel, S. A. Jenekhe, *J. Am. Chem. Soc.* **2003**, *125*, 13656–13657.
- [23] a) S. Shinamura, I. Osaka, E. Miyazaki, A. Nakao, M. Yamagishi, J. Takeya, K. Takimiya, *J. Am. Chem. Soc.* **2011**, *133*, 5024–5035; b) M. Nakano, K. Niimi, E. Miyazaki, I. Osaka, K. Takimiya, *J. Org. Chem.* **2012**, *77*, 8099–8111; c) M. Mamada, T. Minamiki, H. Katagiri, S. Tokito, *Org. Lett.* **2012**, *14*, 4062–4065; d) M. Mamada, H. Katagiri, M. Mizukami, K. Honda, T. Minamiki, R. Teraoka, T. Uemura, S. Tokito, *ACS Appl. Mater. Interfaces* **2013**, *5*, 9670–9677.
- [24] a) L. Pålsson, A. P. Monkman, *Adv. Mater.* **2002**, *14*, 757–758; b) L. Porrès, A. Holland, L. Pålsson, A. P. Monkman, C. Kemp, A. Beeby, *J. Fluoresc.* **2006**, *16*, 267–272; c) A. K. Gaigalas, L. Wang, *J. Res. Natl. Inst. Stand. Technol.* **2008**, *113*, 17–28.
- [25] a) D. D. Kenning, K. A. Mitchell, T. R. Calhoun, M. R. Funfar, D. J. Sattler, S. C. Rasmussen, *J. Org. Chem.* **2002**, *67*, 9073–9076; b) L. Wen, S. C. Rasmussen, *J. Chem. Crystallogr.* **2007**, *37*, 387–397; c) L. Wen, J. P. Nietfeld, C. M. Amb, S. C. Rasmussen, *J. Org. Chem.* **2008**, *73*, 8529–8536.
- [26] a) J. Hu, D. Zhang, F. W. Harris, *J. Org. Chem.* **2005**, *70*, 707–708; b) M. Yamada, Y. Tanaka, Y. Yoshimoto, S. Kuroda, I. Shima, *Bull. Chem. Soc. Jpn.* **1992**, *65*, 1006–1011; c) J. Bolger, A. Gourdon, E. Ishow, J.-P. Launay, *Inorg. Chem.* **1996**, *35*, 2937–2944; d) S. Bodige, F. M. MacDonnell, *Tetrahedron Lett.* **1997**, *38*, 8159–8160; e) G. Conte, A. J. Bortoluzzi, H. Gallardo, *Synthesis* **2006**, *23*, 3945–3947; f) Y. Sun, D. A. Lutterman, C. Turro, *Inorg. Chem.* **2008**, *47*, 6427–6434.
- [27] Gaussian 03, Revision D.02, M. J. Frisch, G. W. Trucks, H. B. Schlegel, G. E. Scuseria, M. A. Robb, J. R. Cheeseman, J. A., Jr., Montgomery, T. Vreven, K. N. Kudin, J. C. Burant, J. M. Millam, S. S. Ivengar, J. Tomasi, V. Barone, B. Mennucci, M. Cossi, G. Scalmani, N. Rega, G. A. Petersson, H. Nakatsuji, M. Hada, M. Ehara, K. Toyota, R. Fukuda, J. Hasegawa, M. Ishida, T. Nakajima, Y. Honda, O. Kitao, H. Nakai, M. Klene, X. Li, J. E. Knox, H. P. Hratchian, J. B. Cross, V. Bakken, C. Adamo, J. Jaramillo, R. Gomperts, R. E. Stratmann, O. Yazyey, A. J. Austin, R. Cammi, C. Pomelli, J. J. Dannenberg, V. G. Zakrzewski, S. Dapprich, A. D. Daniels, M. C. Strain; O. Farkas, D. K. Malick, A. D. Rabuck, K. Raghavachari, J. B. Foresman, J. V. Ortiz, Q. Cui, A. G. Baboul, S. Clifford, J. Cioslowski, B. B. Stefanov, G. Liu, A. Liashenko, P. Piskorz, I. Komaromi, R. L. Martin, D. J. Fox, T. Keith, M. A. Al-Laham, C. Y. Peng, A. Nanayakkara, M. Challacombe, P. M. W. Gill, B. Johnson, W. Chen, M. W. Wong, C. Gonzalez, J. A. Pople Gaussian, Inc., Pittsburgh PA, **2003**.

Received: April 12, 2014

Published online on July 30, 2014